EUROPEAN ORGANIZATION FOR NUCLEAR RESEARCH
European Laboratory for Particle Physics

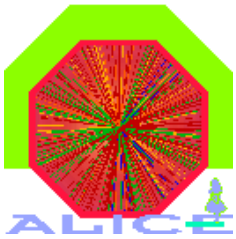

Internal Note/
ALICE reference number
ALICE-INT-2005-031 version 1.0
Institute reference number
[-]
Date of last change
June 2005

Two Track Effects at ALICE

Authors:

Piotr Krzysztof Skowroński

CERN, Geneva, Switzerland and Warsaw University of Technology, Faculty of Physics, Warsaw, Poland

Jan Pluta
Grzegorz Gałązka
Michał Olędzki
Hanna Gos

Warsaw University of Technology, Faculty of Physics, Warsaw, Poland

Ludmila Malinina

Joint Institute for Nuclear Research, Russia

Contents

1 Introduction

It is expected that a few thousands of particles per unit of rapidity will be emitted in heavy ion collisions at LHC energies. It will create a very dense pattern of hits in the detectors. Possible effects of hit sharing and track overlapping can be especially dangerous for the analysis of particle correlations at small relative momenta (close velocities). A detailed simulations are necessary to eliminate the influence of systematic distortions, as the statistical errors will be negligible in most cases.

A dedicated software has been developed for analysis of momentum correlations at ALICE [2][3][4]. We present here some specific points of the correlation studies and the results obtained for simulated and reconstructed correlation effects as well as the conclusions coming from the comparative analysis. The first goal of this work is to verify the possibility of ALICE detection system in measuring different features of particle correlations and other signals depending on the two particle spectra. The second one is to develop the software tools that could be directly applied for the analysis of the real data in future.

The two tracks effects change the registration probability of two-particle system. Three main forms of these effects can be distinguished:

1. **merging** - registration of one particle instead of two, usually due to track overlapping,

2. **splitting** - reconstruction of two particles on the base of the data belonging to one particle,

3. **distortion** - changes of the measured particle parameters due to the proximity of an another one.

The proximity of the other track can both, worsen the resolution and induce a systematic shift, due to increasing probability of the cluster assignment belonging to the neighboring track. It also can induce the particle type misidentification.

Variables that are the most affected by the two track effects are the ones used in the correlations analyses. It is because the signal is observed for the particles close in the momentum space what indicates closeness in the detector, which in turn has always a finite granularity and separation power.

Clearly, the effects of two track resolution play an important role in the kinematic region of small relative momenta for identical particles. It is less important for nonidentical ones. Indeed, particles with different charges are deviated by the magnetic field in different directions. Particles with different masses emitted with small relative momenta in the two-particle rest frame have close velocities but different momenta in the laboratory system and are differently deviated by the magnetic field.

2 The basic principles and variables of the close velocity correlations

Two hadrons interact strongly and eventually electromagnetically if both counter-partners have non zero electric charge. These Final State Interactions (FSI) are as more pronounced as the emitted particles have closer velocities and are closer in space. If they are distinguishable (i.e. not identical) it is possible to measure the sequence of the emission with the FSI induced correlations. If they are identical, additionally the quantum statistics plays a role and additional correlations appear.

In the both cases the correlation function gives the information about the so called homogeneity length, which is the average dispersion around the point of the highest emissivity. It is impossible to find unambiguously all the four dispersions (three spacial and one temporal) and an additional model assumption is always required. Hence, in the non-identical analysis we can not distinguish if both particle types are emitted at the same time and the points of the highest emissivity do not coincide or if particles of the first type are emitted earlier from the same point then those of the second type.

The most important variable is the length of velocity difference vector $2K^*$. If particles have the same mass it is equivalent to the invariant momentum difference Q_{inv}. The vector can be decomposed to the following components, see Fig.1:

- *long* parallel to beam
- *side* perpendicular to beam and pair momentum K
- *out* perpendicular to *long* and *side*

The most adequate frame is the so called Longitudinally Co-Moving System (LCMS) where velocity components in beam (longitudinal) direction are equal. The LCMS frame is used through out this note.

Note also that for small opening angles the components *long* and *side* are approximately proportional to the relative polar ($\Delta\theta$) and azimuthal ($\Delta\phi$) angles, respectively. The *out* component is determined by the difference of the absolute values of transverse velocity and depends on the tracks curvature.

3 Correlation simulations

None of the existing event generators is able to simulate relativistic heavy ion collision with correlations arising from quantum statistics and final state interaction effects. These effects are of the quantum origin and require appropriate propagation of the wave functions while generators normally work with the probabilities. Moreover, the proper quantum calculation requires solving n! equations, where n is number of particles in an event, what is nowadays impossible to perform within a finite time.

Below are presented the two existing ways which allow to circumvent the problem.

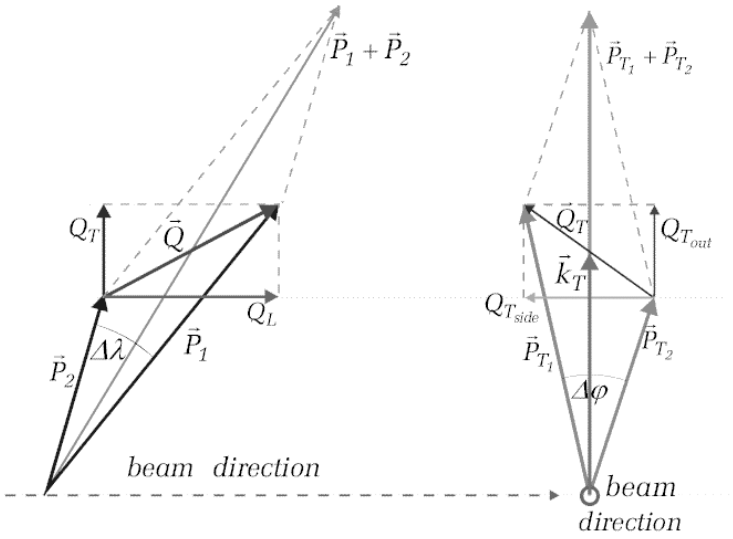

Figure 1: Basic kinematic variables of correlation analysis

3.1 HBT processor

Correlation functions constructed with the data produced by any event generator are normally flat in the region of small relative momenta. In order to add the effects of the two particle correlations we have applied the HBT-processor "after-burner" [5]. It randomly reshuffles particle momenta about small values up to the moment the obtained correlation is sufficiently close to the required shape. The HBT processor is an excellent tool to verify the influence of different experimental factors on the shape of the correlation function.

It is not applicable to generate the dynamic effects by multiple application of HBT processor for different intervals of P_t and y. For such cases we have applied the method of weights described below.

3.2 The weighting algorithm

In this approach the correlation function is constructed by calculating weights reflecting the particle correlations resulting from the quantum statistics and the final state interactions. The weight is attributed to a pair of selected particles and it depends on the space-time coordinates of the emission points and on the four-momenta of both particles.

The correlation function is obtained as a ratio of weighted to unweighted distributions, taken as a function of any variable reflecting the particle relative momentum: Q_{inv} or its components (f.g. $(out, side, long)$).

In this way the two-particle correlation function is created pair-by-pair for different types of two-particle systems, identical or nonidentical, taking into account all the details of particle emission process included in the event generator: expansion, flow, resonance production etc. A parameterization of the correlation function is not necessary. This

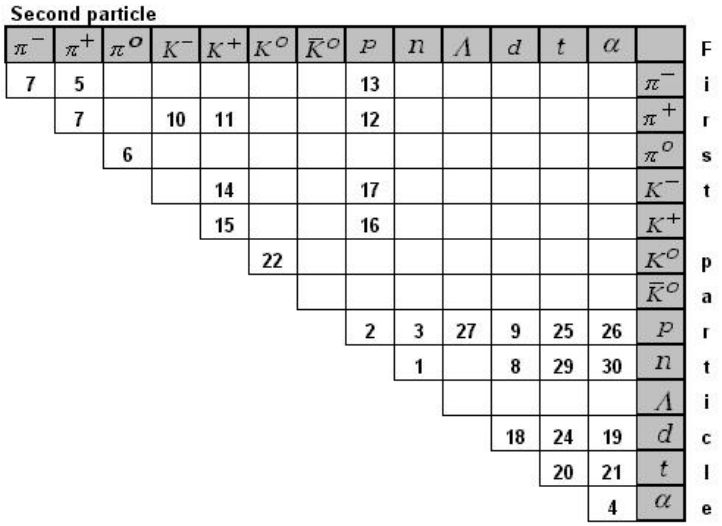

Figure 2: A list of two-particle systems for which the weights can be calculated with the software used at ALICE. The numbers correspond to pair numbering in the applied computer code "FSIWLL".

approach can be applied as an after-burner for any dynamical model giving the freeze-out coordinates of the emitted particles: RQMD, NEXUS, UrQMD etc.

The analyzed data were simulated with the Hijing generator that does not give the freeze-out coordinates and they are needed to be randomized before or during the analysis step according to some distribution. Actually, the shape the correlation function depends only on the distribution of the distance 4-vector between particles. In both of the cases studied in this note, i.e. Gaussian shapes of the Q_{inv} CF and $Q_{out}Q_{side}Q_{long}$ CF, it was the easiest to attribute the distances between each pair separately during the mixing. In the first case the distributions in out, side and long must be Gaussian in the pair rest frame. In the second case these distributions must be Gaussian in LCMS.

4 Expected correlation effects

Before starting simulations for any selected values of the space-time parameters let us realize the limits of correlation effects expected for ALICE.

Fig. 3a presents the form of correlation function for the pairs of positively charged pions emitted from the Gaussian source of indicated sizes: 3,5,10,20 fm. The complete calculation have been performed including QS, strong and Coulomb FSI. For the sake of comparison the shapes of correlation functions containing only the QS effect are presented for smallest 3 fm and largest 20 fm sizes.

For the most expected size of the order of 6 – 8 fm the Q_{inv} region where the corre-

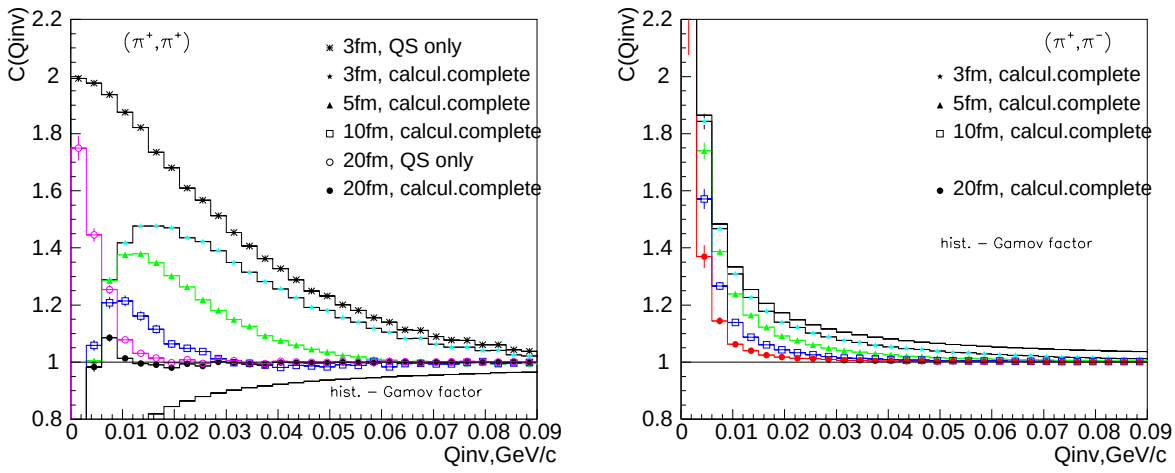

(a) (b)

Figure 3: Correlation functions for a) $\pi^+\pi^+$ and b) $\pi^+\pi^-$ systems and for sizes indicated in the figure. The intercept parameter $\lambda = 1$ was assumed.

lation functions differ from unity is less than 50 MeV/c and the height is on the level of 1.2 despite the assumption of totally chaotic source (the chaocity parameter λ equal to one). For the size of 20 fm (the full points) the effect of the Coulomb repulsion almost completely equilibrate the QS positive correlations giving very small effect in the region about 10 MeV/c. The Coulomb effect should be in this case much larger than the effect itself (see the open circles). It is clear that the traditional approach in which Coulomb effect is treated as a correction could not be applied in this case. Note also that the long range Coulomb effect can reflect different sizes than QS ones. Although such large size is doubtful in the light of last results from RHIC, it is evident that the expected effects should not be located at the edge of experimental possibilities.

Fig. 3b shows correlation function for the pairs of different charge pions. In this case the Coulomb effect determines the shape of correlation function. The behavior of Gamow factor is indicated as a reference. Due to the lack of QS effect and because of large value of the Bohr radius for two-pion system the sensitivity to the sizes are weaker than for identical pions. However, for larger sizes this difference becomes smaller and for the radius of 20 fm the correlation effect for nonidentical pions exceeds that for identical ones. The correlation effect is localized in the region of very small relative momenta but note that in the case of (π^+, π^-) pairs the problem of double track resolution should be less important, as different charge particles are deviated in different directions by the magnetic field.

The next example, Fig. 4a, shows the correlation function for the system of particles with different masses, $\pi^+ p$. As the Bohr radius is substantially smaller in this case, the

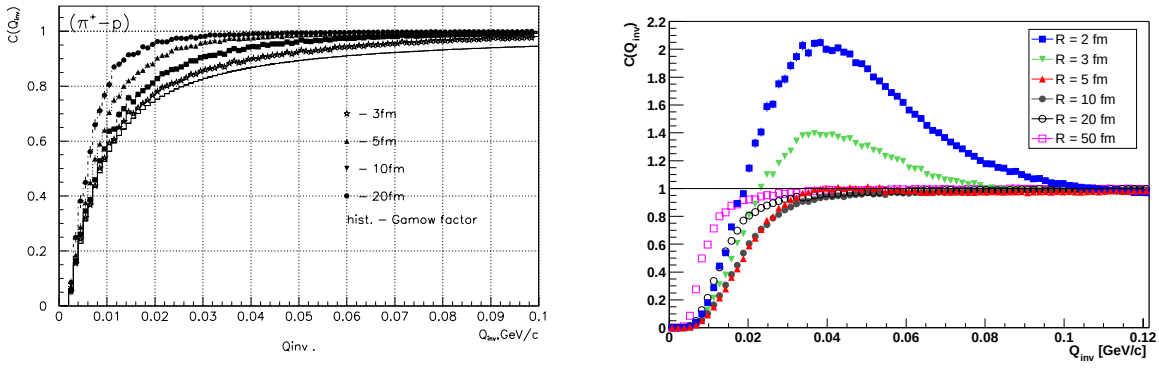

(a) (b)

Figure 4: Correlation functions for a) $\pi^+ p$ and b) pp systems and for sizes indicated in the figure. The intercept parameter $\lambda = 1$ was assumed.

sensitivity to the sizes are larger than for the system of two pions. Although the sign of particle charges is the same here, the curvature in magnetic fields for pions and protons with the same velocity is very different due to large difference in masses.

The last example, Fig. 4b, presents the correlation function for two protons. For this system of two fermions the effect of QS resulting from Fermi-Dirac statistics leads to negative correlations coming to the value 0.5 for the zero value of Q_{inv}. If the sizes are relatively small the interplay between attractive strong interaction and the Coulomb repulsion gives the broad maximum located about Q_{inv} of 40 MeV/c. For larger radii the size dependence is relatively week. The curve for unrealistic value of 50 fm is shown to demonstrate it.

5 The data and the analysis

In this note we show the results obtained with the data produced during Physics Data Challenge 2004 (PDC04). The most detailed available simulation was used. Events were generated with the Hijing generator. We concentrate here on the most central events (impact parameter range from 0 to 2 fm) yielding the average multiplicity of the order of 6000 charged particles per unit of rapidity. To simulate the correlation effects we make use of the weighting algorithm. In order to verify the obtained results 500 events were produced with correlations simulated by HBT processor.

The detailed description of the reconstruction code can be found in [2] and [3]. The tracks reconstructed with the central barrel detectors are used, i.e ITS, TPC, TRD, TOF and HMPID with the parameters obtained with the vertex constraint. The particle is considered being of a given type if its PID probability is bigger then 50%.

In case of the identical particle analysis we always assume the lack of the Final State Interactions. This is justified because in the simulation we perfectly know the shape of the correlation induced by FSI and the correction for these effects does not bring any uncertainties. Of course, in the experimental data analysis the exact contribution is unknown, and proper handling is the major problem which brings the most significant contribution to the systematic error.

6 Event selection for the background mixing

It is known that events with very similar properties should be mixed in order fill a denominator of correlation function. Otherwise correlations due to a global event characteristics might be exposed. In this analysis we use only central events which have similar particle multiplicities and have no flow. Hence there was no necessity of grouping events according to the number of particles or the event plane, which is necessary when analyzing real data.

We have observed that obtained correlation functions exhibit influence of the detector topology. It is caused by the mixing events having the primary vertex at different positions. Some relative momenta are less efficiently reconstructed due to the detector segmentation, f.g. gaps between ITS modules or TPC sectors, see example schema in Fig.5. The influence of these inefficiencies on the relative momentum distribution is changed if the events have different primary vertex position, namely they are smeared out. Of course, all these inefficiencies are always present in numerators. In consequence they are visible in the correlation functions.

We have observed the effect related to the pixel length in SPD's. Position of the point where the track passes detector is always assumed to be at the center of a cluster. Since most of clusters are composed of only one pixel, the reconstructed coordinates correspond to the centers of pixels. In the consequence some values of Q_{long} are more preferable then others. Hence, it is necessary to mix events having z position of the primary vertex smaller that the half width of the pixel, i.e. $225\mu m$. In our analyses we have grouped all events according to the z vertex position, and only events falling into single bin were used in event mixing. We have chosen the width of the bin 100μm that allowed to remove the effect.

In the case of HBT variables the effect is smeared out when analysis is integrated over sufficiently large range of transverse momentum (pairs of tracks having the same open angle but different momenta yield different Q values). Hence, the necessity of the event sorting according vertex position can be questioned. However, it is better to be on the safe side and use the technique proposed above. Especially that it is very easy to implement it, it does not have any drawbacks on statistics or processing time and the appropriate tools that automates it are being developed (the tag database).

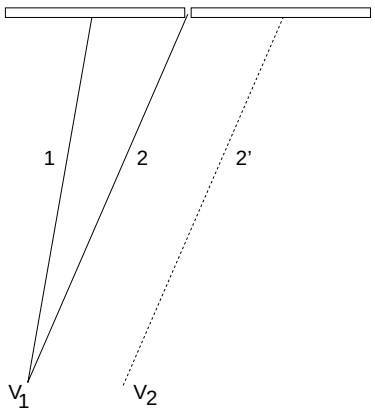

Figure 5: Schema of the effect leading to the correlations due to the Silicon Drift Detector topology. Squares are the pixels, solid lines are tracks from the event having primary vertex at V_1, dashed line from from V_2. Pairs like 1-2 are relatively less efficiently reconstructed what reflects itself in the shape of numerators. It is not the case for denominators if pairs like 1-2' are used.

7 Track splitting

We have implemented the anti-splitting cut developed for the STAR experiment. It utilizes the binary hit-map which is a bit-vector that has 1 on the n'th field if a given track has a cluster on a n'th padrow of TPC. For each pair of tracks a quality factor $F_{Quality}$ is calculated using the following formula

$$F_{Quality} = \frac{\sum_{n=1}^{N_{padrows}} A(n)}{\sum N_{Clust}} \tag{1}$$

where:

$$A(n) = \begin{cases} -1, & if\ both\ tracks\ have\ cluster\ on\ padrow\ n \\ 0, & if\ neither\ track\ has\ cluster\ on\ padrow\ n \\ 1, & if\ only\ one\ track\ has\ cluster\ on\ padrow\ n \end{cases} \tag{2}$$

where $N_{padrows}$ is number of TPC padrows and $\sum N_{Clust}$ is total number of clusters for both tracks. It can take values in the range $[-0.5, 1]$. A value close to 1 describes a pair of tracks that has high likelihood of being a splitted track f.g. case 2) and 3) in Fig.6.

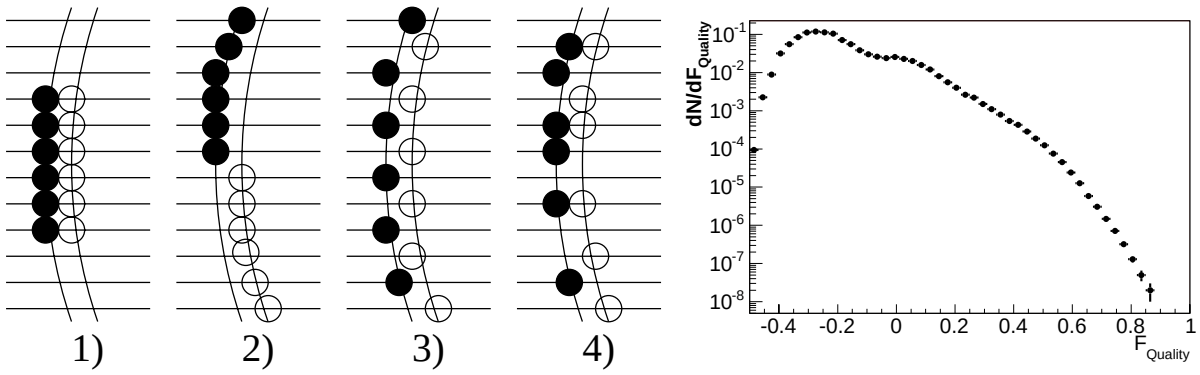

(a) (b)

Figure 6: a) Four examples of clusters attributed to two tracks: Full circles are clusters assigned to first track and open circles are clusters assigned to the second one. 1) $F_{Quality} = -0.5$, 2) and 3) $F_{Quality} = 1$ and 4) $F_{Quality} = 0.25$. b) Obtained normalized distribution of $F_{Quality}$.

However, it turned out to be void for ALICE because the tracking software already performs all the possible checks and removes all splitted tracks in TPC. In Fig. 6b the normalized distribution of $F_{Quality}$ is presented. The STAR experiments rejects all pairs with the factor above 0.6. In the our case the fraction of pairs over this values is smaller then 10^{-5}.

This is also supported by the fact that we do not observe any artificial rise of the correlation function for very small momentum differences if no cuts are applied.

However, it is not true if one includes tracks reconstructed by the stand alone ITS tracking (not to be mistaken with the *neural* stand alone ITS tracking mentioned in one of the next section). We have found the strong positive correlation for very small Q values when these tracks were included in the analysis. It indicates that the large fraction of the tracks reconstructed by this tracking are already found by the standard tracking. Tracks reconstructed only by the ITS stand-alone tracking, as it was used in PDC04, should not be used for HBT analyses.

8 Track Merging

8.1 Identical pions

As it was explained in section ref{sect:ResolutionStudy} track merging introduces artificial negative correlation at small relative momentum. In order to reconstruct correct radii it is important to remove this effect.

In general, the track merging is expected to depend on momentum because the close track reconstruction efficiency depends on the level of multiple scattering. In the acceptance of the ALICE central barrel momentum can be roughly approximated by transverse momentum. Since it was easier to work with transverse momentum, we have done the study for two ranges of p_t: up to 500 MeV/c and above this value. The limited statistics of the simulated Monte Carlo Data (20000 events) has not allowed to increase the number of bins.

The radii measured at lower energies are of the order of 6 fm [8]. We have decided to assume the Gaussian source with all radii equal to 8 fm and intercept parameter $\lambda = 1$. The Final State Interactions were neglected to simplify the quantitative analysis. All the correlation functions presented in this section are simulated using these parameters unless explicitly stated otherwise.

The obtained correlation functions, without any pair cut, are shown in Fig.7a. Merging effect is clearly visible at small relative momenta (see also Fig.9). Note that the effect in *side* and *long* it is much narrower (15 MeV) then in *out* (150 MeV). By comparing these functions we can learn the influence of different effects on the shape of the correlation. Reconstructed correlation function (red up-pointing triangles) is influenced by all the effects, i.e. merging, resolution and PID impurity. The function without a correlation effect simulated (green down-pointing triangles) shows the merging effect solely. The one constructed only with particles having correctly reconstructed PID gives the information about influence of the PID impurity. The last one (blue dots) is made using the simulated momenta and only for particles having correct PID. Its comparison with the previous one displays the influence of the finite resolution.

In real data analysis the presence of the merging effect is detected with non-zero value $R_{outside}$, when fitting 3-dimensional correlation function for the central events with the following formula:

$$C(Q_{out}, Q_{side}, Q_{long}) = 1 + \lambda \exp(-Q_{out}^2 R_{out}^2 - Q_{side}^2 R_{side}^2 - Q_{long}^2 R_{long}^2 - 2Q_{out}Q_{side}R_{outside}^2) \quad (3)$$

This condition results from the symmetry constraints [7], [8]. Moreover, the track merging affects positively charged particles in a different way than negatively charged ones, see Fig. 7b and 9a. Namely, pairs with the negative sign of $Q_{out} \cdot Q_{side}$ are more vulnerable in the first case (the merging effect is more pronounced in the 2nd and 4th quadrant of Fig.9a). For the second case pairs with the positive $Q_{out} \cdot Q_{side}$ are more influenced, so the merging is larger in 1st and 3rd quadrant of $Q_{out}Q_{side}$ correlation function. In consequence the correlation function is tilted if the merging is present and the tilt is opposite for positively

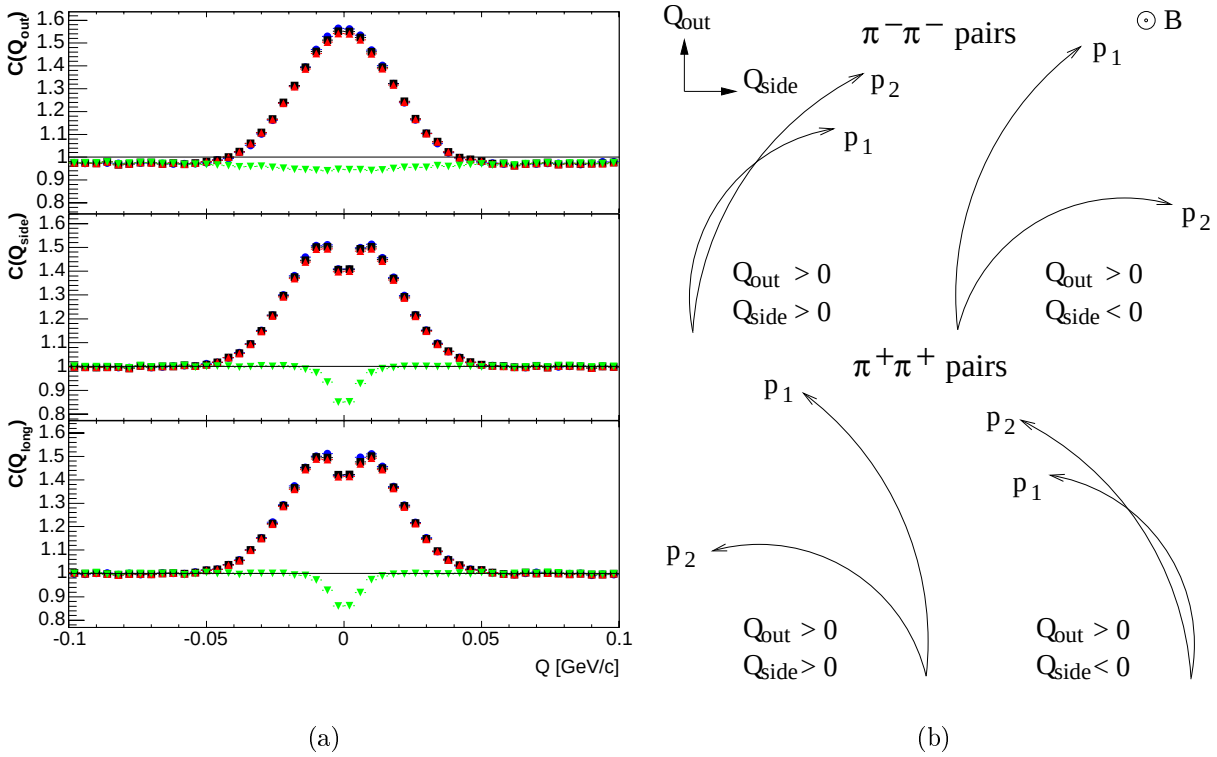

(a) (b)

Figure 7: a) Projection of the $\pi^+\pi^+$ correlation function for other components smaller then 20 MeV. No cuts applied. Red up-pointing triangles are the reconstructed functions, black squares are only for particles with correctly identified PID, blue dots are created using generated momenta and perfect PID, green down-pointing triangles are without simulated Bose-Einstein effect.
b) Possible trajectory topologies of pairs with the same sign of the electric charge and their relation to the sign of $Q_{out} \cdot Q_{side}$.

charged pairs then for negatively ones and this results in opposite sign of the fitted $R_{outside}$ if the track merging is present. Of course the situation would be reversed if the direction of the magnetic field would be altered.

We have introduced the anti-merging cut which rejects pairs of tracks that have smaller average distance while they fly though the TPC volume than the given threshold (d_{min}). The average distance is calculated at 10 equidistant radii (every 15 cm) starting from the inner surface of TPC, i.e. 84.1 cm. Track coordinates are computed assuming the helix shape of a track with the parameters as they are reconstructed at inner surface of TPC.

The assumption about helix shape of a track is justified since multiple scattering is negligible inside TPC. In order to find the appropriate threshold value of the cut the correlation function of Q_{inv} versus average separation is constructed. Track merging is clearly visible at small Q_{inv} (see Fig.9). However, one should keep in mind that these two properties are strongly correlated, since identical particles emitted with small relative momenta must have a close trajectories.

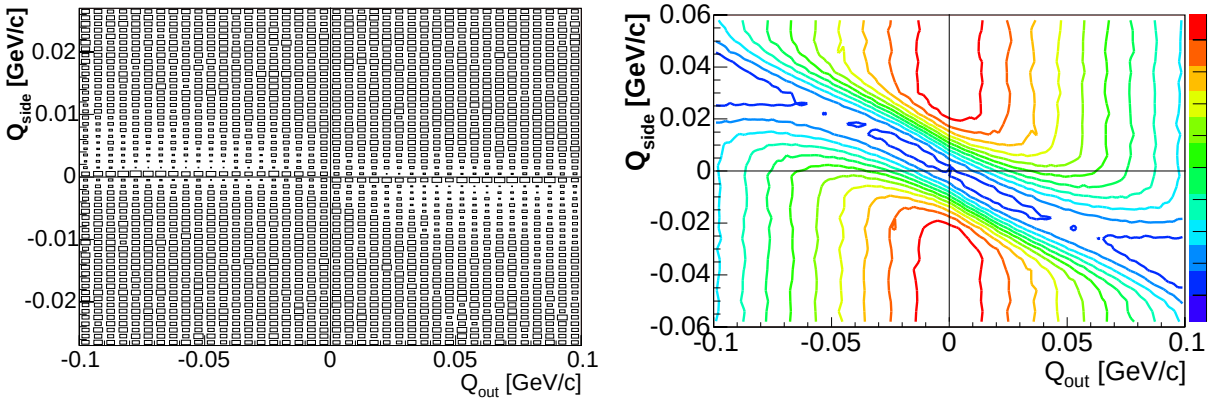

(a) (b)

Figure 8: a) $\pi^+\pi^+$ $Q_{out}Q_{side}$ correlation function and b) and its denominator for $p_t < 500$ MeV. All tracks having average separation in TPC below 6 cm were rejected.

We have analyzed the data with several threshold values, see Fig.10. As it can be seen in Fig.8 and 10 it reduces the merging effect, but does not remove it completely. As it can be learned from the comparison of plots a) and b) in Fig.8, the remaining effect is situated at different region of $Q_{out}Q_{side}$ space than the cut affects.

This implies that the originally observed track merging is caused by the track reconstruction inefficiency in ITS, because the tracks potentially merged in TPC renders Q_{out} and Q_{side} situated along the valley visible in Fig.8b and the remaining merging is located at smaller values of Q_{side} (Q_{side} is related to the azimuthal angle between two tracks). Hence, the merging occurs for pairs of tracks that cross before TPC.

We have constructed a 3D correlation function: Q_{inv} versus spacial track separation in z and $r\phi$ at a given ITS layer. This lets us determine what are distances between trajectories

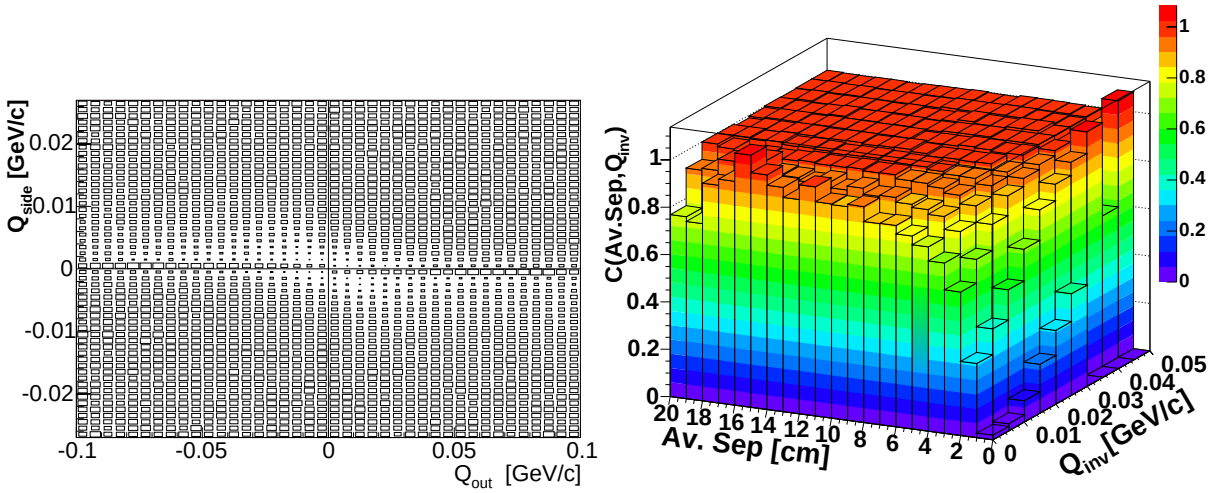

(a) (b)

Figure 9: a) $Q_{out}Q_{side}$ correlation function ($Q_{long} < 20$ MeV). b) Average separation in TPC versus Q_{inv} correlation function. $\pi^+\pi^+$, $p_t < 500$ MeV. No correlation effect simulated.

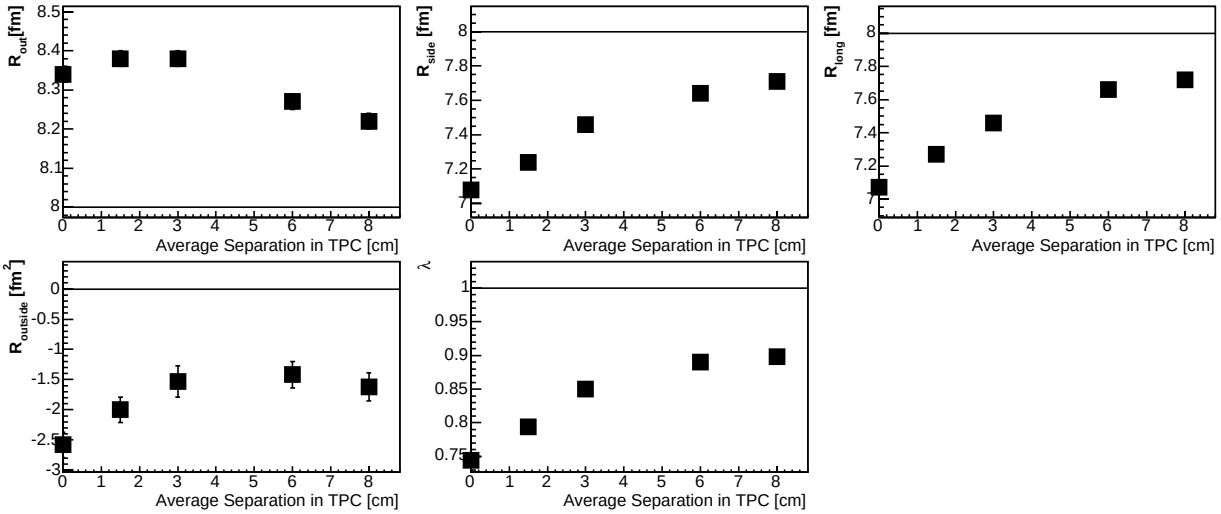

(a)

Figure 10: Extracted source parameters in function of the minimum allowed average separation in TPC for $\pi^+\pi^+$ and $p_t < 500$ MeV.

below which two tracks are reconstructed less efficiently. Positions of a track are calculated assuming helix trajectory. For the 3 most inner layers parameters reconstructed at vertex are used, while for the outer ones, parameters at the inner surface of TPC are taken. Two dimensional projection for the innermost layer is presented in Fig.11. These correlation functions indicate that the cuts summarized in Table 1 should be applied additionally to the TPC average separation cut (we chose $d_{min} = 6$ cm).

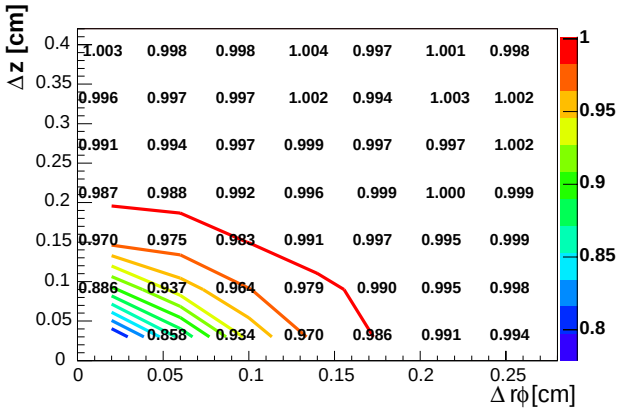

Figure 11: Correlation function of the spatial separation at the first layer of ITS in the case no cut is applied. Lines represent the isolines. No correlation effect simulated.

Since the reconstruction is done in the incremental way (tracks are always prolongated from one detector to the another one) we are not able to disentangle different sources of the close track reconstruction inefficiency. It means that if we observe an inefficiency at one of the detectors (f.g. the average separation in TPC) we can not disentangle if this detector is inefficient this way or it is caused by some other detector (f.g. in ITS) and it is only such reflected in this observable.

Hence, first we have verified if the effect could be removed using the separation cut on the first layer of ITS solely. Obtained results are shown in Fig.12. From this plot, and also from the detailed analysis of other correlation functions it is clear that a combined cut is needed. It has to reject particles passing too close to each other at any layer of ITS (threshold values in Table 1) and are also sufficiently far in TPC (average separation larger then 6 cm).

After applying the cuts correlation function is almost free from the merging effects comparing to the one obtained without any cuts. The fit gave the following parameters: $R_{out} = 7.89 \pm 0.03$, $R_{side} = 7.87 \pm 0.02$ fm, $R_{long} = 7.89 \pm 0.02$ fm, $R^2_{outsides} = -0.50 \pm 0.23 fm^2$, $\lambda = 0.923 \pm 0.005$ and $\chi^2/NDF = 1.01$.

Further we have examined how the parameters change with the anti-merging cut strength. We define the threshold values listed in Table 1 as the base, and change them by the multiplicative factor (0 means no cuts). Results are presented in Fig.13. This figure indicates that these values are optimal because making them 50% looser increase considerably $Q_{outsides}$ (although the other parameters almost do not change), and increasing them

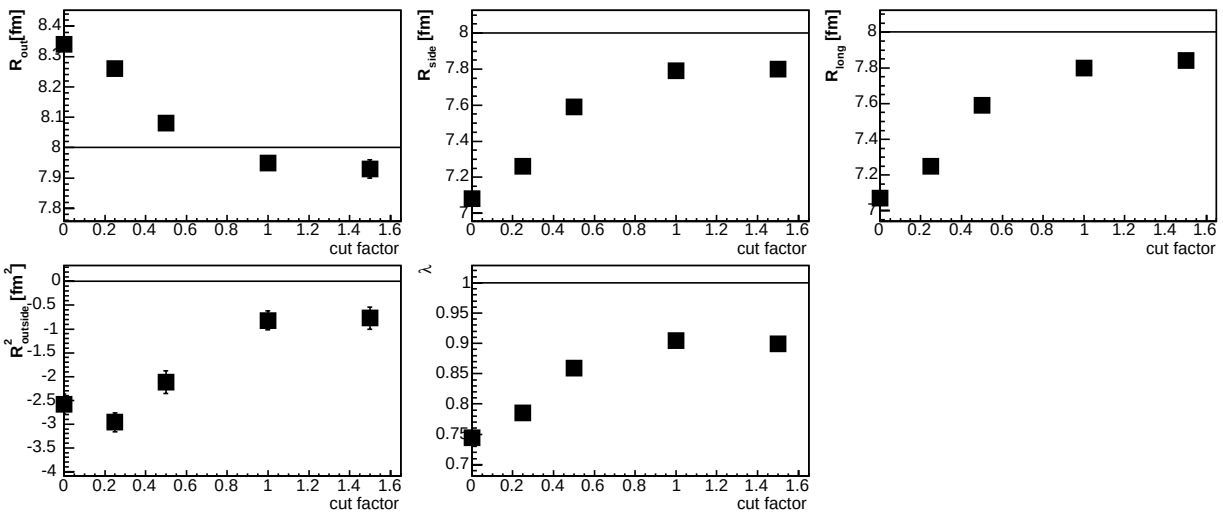

(a)

Figure 12: Extracted source parameters as a function of the SPD1 anti-merging cut strength for $\pi^+\pi^+$ and p_t's up to 500 MeV. Unity corresponds to 1.5 mm in $r\phi$ and 2 mm in z and both are multiplied by the $factor$.

Layer	$r\phi$ [mm]	z [mm]
1 (SPD1)	1.5	2
2 (SPD2)	3	3
3 (SDD1)	6	8
4 (SDD2)	12	12
5 (SSD1)	15	15
6 (SSD2)	15	15

Table 1: Chosen values of the anti-merging cut in ITS for the low momentum range $\pi^+\pi^+$.

about 50% significantly removes the signal, what expresses itself in increasing error of Q_{out}. This figure also suggests that the discrepancies from the simulated values are caused by the resolution and not perfect PID effects, that will be discussed in the following section.

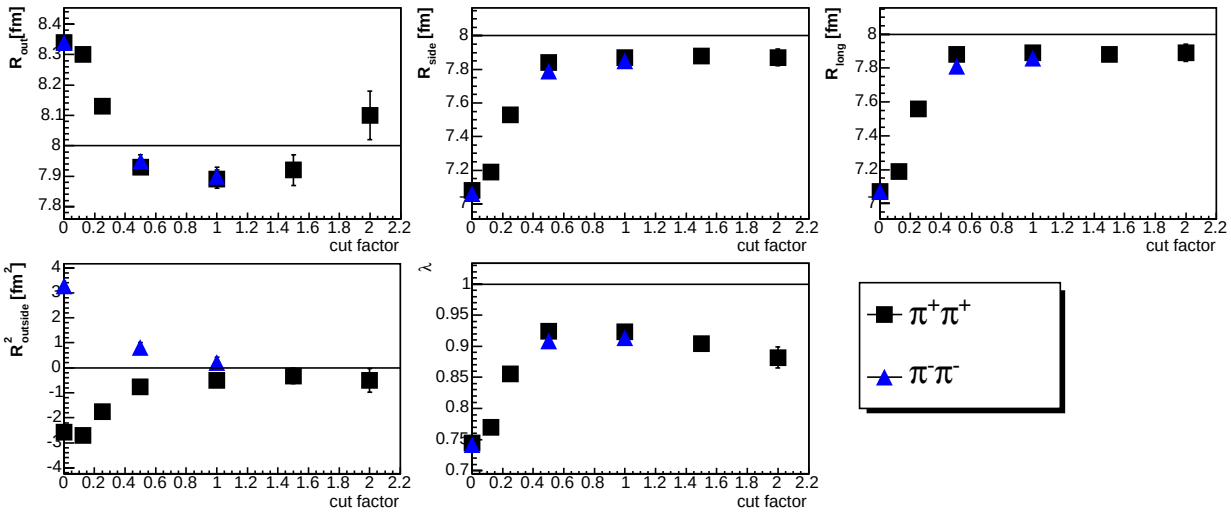

(a)

Figure 13: Extracted source parameters in function of the anti-merging cut strength for $\pi^+\pi^+$. Unity corresponds to the set listed in Table 1 and the average separation in TPC equal to 6 cm. All threshold values are multiplied by the factor.

In order to estimate the systematical errors we have studied how the extracted parameters change if the cut threshold values are variated. We have increased and decreased about 50%

1. all threshold values
2. only at the innermost layer of ITS (SPD1)
3. the average separation in TPC
4. all the threshold values in ITS in z direction
5. all the threshold values in ITS in $r\phi$ direction

In Table 2 are presented the results. None of them has any dramatic influence on the obtained parameters. Their spread defines the systemic errors and the resulting values are listed in Table 5.

Further, analysis was repeated for the remaining transverse momentum range, i.e. over 500 MeV. In Fig.14a is presented the relative efficiency of the pair reconstruction in function of the spatial separation at the first layer of pixel detectors. The region where the

Type of cut	R_o [fm]	R_s [fm]	R_l [fm]	$R^2_{os}[fm^2]$	λ
standard	7.90 ± 0.03	7.87 ± 0.02	7.89 ± 0.02	-0.51 ± 0.23	0.923 ± 0.005
0.5 standard	7.94 ± 0.02	7.85 ± 0.02	7.89 ± 0.02	-0.77 ± 0.20	0.924 ± 0.003
1.5 standard	7.92 ± 0.04	7.87 ± 0.03	7.88 ± 0.03	-0.32 ± 0.31	0.903 ± 0.009
0.5 SPD1	7.87 ± 0.03	7.86 ± 0.02	7.91 ± 0.02	-0.41 ± 0.23	0.920 ± 0.005
1.5 SPD1	7.88 ± 0.03	7.85 ± 0.02	7.87 ± 0.02	-0.27 ± 0.25	0.907 ± 0.006
0.5 TPC	7.92 ± 0.03	7.88 ± 0.02	7.89 ± 0.02	-0.61 ± 0.22	0.924 ± 0.005
1.5 TPC	7.89 ± 0.03	7.88 ± 0.02	7.88 ± 0.02	-0.41 ± 0.25	0.919 ± 0.005
0.5 in $r\phi$	7.87 ± 0.02	7.88 ± 0.02	7.90 ± 0.02	-0.30 ± 0.21	0.927 ± 0.004
1.5 in $r\phi$	7.89 ± 0.03	7.90 ± 0.02	7.86 ± 0.02	-0.40 ± 0.27	0.912 ± 0.006
0.5 in z	7.90 ± 0.02	7.85 ± 0.02	7.88 ± 0.02	-0.45 ± 0.22	0.921 ± 0.004
1.5 in z	7.88 ± 0.03	7.84 ± 0.02	7.91 ± 0.02	-0.42 ± 0.24	0.912 ± 0.006

Table 2: Stability of the fitted HBT parameters on variation of the cuts for $\pi^+\pi^+$ and p_t below 500 MeV. Standard corresponds to the set listed in Table 1 and TPC anti-merging cut equal 6 cm. See text for details.

inefficiencies occur has different shape comparing to the low p_t case. In order to remove the merging effect with the same type of cut (i.e. rejecting all points inside a rectangle) it is necessary to apply such a large threshold values, so the HBT signal is completely removed. Hence, it is necessary to introduce more sophisticated cut setting. We have decided to apply the set of three cuts that are defined in the three first rows of Table 3.

We have analyzed data only with the anti-merging cut set at first layer of ITS. As expected, the merging effect was not entirely removed. In Fig. 14b is presented the average separation in TPC versus Q_{inv} correlation function which demonstrates the necessity of applying the cut on the average separation. We chose the threshold value equal to 3 cm. Additionally, we have decided to use cuts on the remaining layers of ITS that are listed in Table 3.

Fitted parameters to the obtained correlation functions and their stability on the cuts threshold values can be learned from Figure 15 and Table 4. Resulting systematical errors are listed in Table 5.

8.2 Non-identical pions

On the first sight the track merging effect should not be present for different charge particle systems, because such a particles are bended in the opposite directions by the magnetic field. However, it may happen that their trajectories cross inside detector (see Fig.16), what leads to the lower reconstruction efficiency for such tracks and in consequence to the artificial correlations. And indeed, we have observed such an effect.

As it is illustrated in Fig.16, pair of tracks having opposite sign of a charge can form

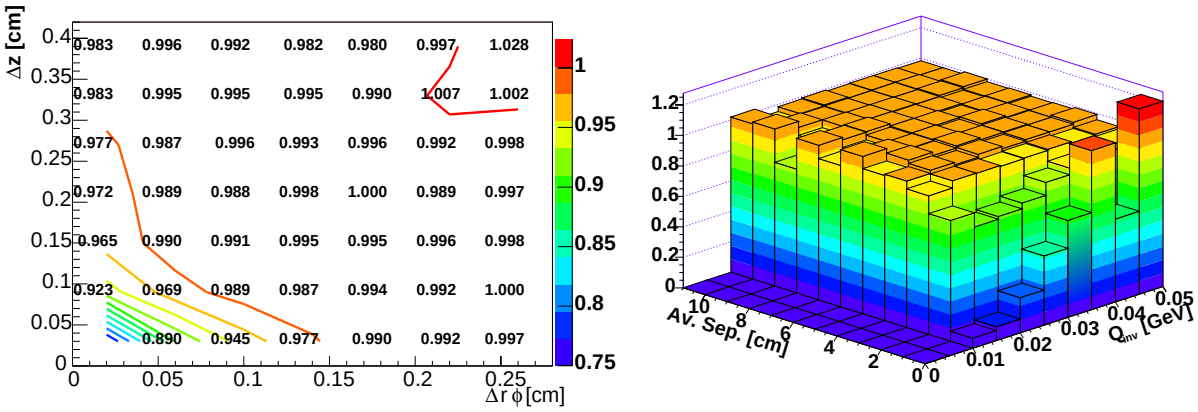

(a) (b)

Figure 14: a) Correlation function of the spatial separation at the first layer of ITS in case no cuts are applied. b) Average separation in TPC versus Q_{inv} correlation function with SPD1 cuts applied. p_t's over 500 MeV.

Layer	$r\phi$ [mm]	z [mm]
1 (SPD1 cut 1)	0.75	1
1 (SPD1 cut 2)	0.45	3
1 (SPD1 cut 3)	1.2	0.6
2 (SPD2)	1.2	1.2
3 (SDD1 cut 1)	1	8
3 (SDD1 cut 2)	3	2
4 (SDD2)	5	6
5 (SSD1)	6	8
6 (SSD2)	6	8

Table 3: Chosen values of the anti-merging cut in ITS for the high momentum range.

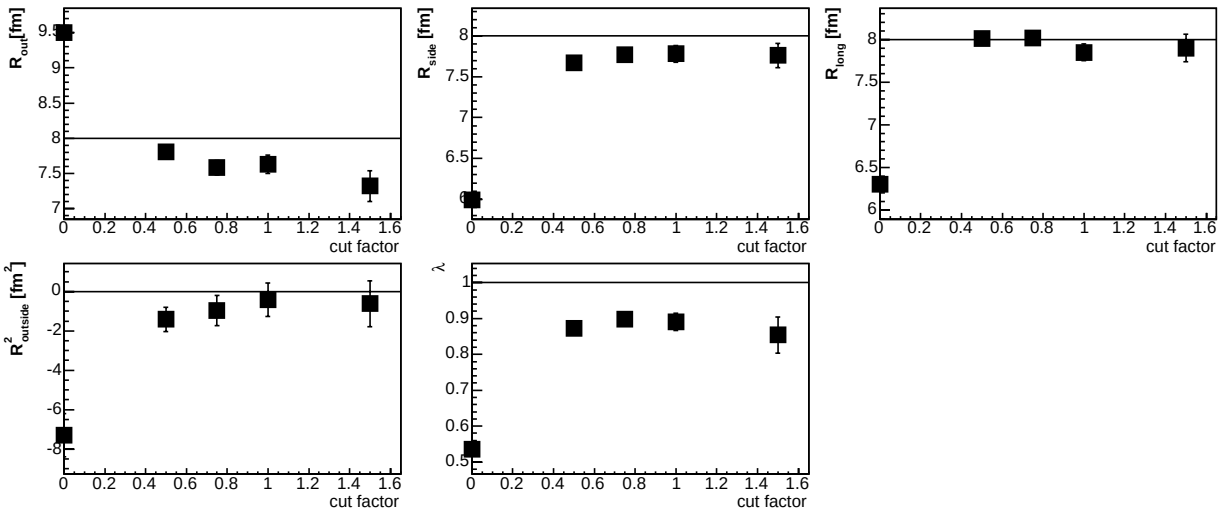

(a)

Figure 15: Extracted source parameters in function of the anti-merging cut strength. Unity corresponds to the set listed in Table 3 and the average separation in TPC equal to 3 cm. All cut values are multiplied by the $cutfactor$. $\pi^+\pi^+$ p_t's over 500 MeV.

Type of cut	R_o [fm]	R_s [fm]	R_l [fm]	$R_{os}^2[fm^2]$	λ
standard	7.63 ± 0.13	7.78 ± 0.10	7.85 ± 0.10	-0.42 ± 0.85	0.891 ± 0.024
0.5 standard	7.81 ± 0.08	7.67 ± 0.06	8.01 ± 0.06	-1.41 ± 0.62	0.873 ± 0.012
0.75 standard	7.58 ± 0.10	7.77 ± 0.08	8.02 ± 0.08	-0.96 ± 0.77	0.898 ± 0.017
1.5 standard	7.32 ± 0.22	7.76 ± 0.15	7.90 ± 0.16	-0.62 ± 1.16	0.854 ± 0.050
0.5 SPD1	7.49 ± 0.11	7.75 ± 0.09	7.98 ± 0.09	-0.51 ± 0.81	0.893 ± 0.019
1.5 SPD1	7.46 ± 0.20	7.62 ± 0.13	7.62 ± 0.15	-1.50 ± 1.07	0.825 ± 0.042
0.5 TPC	7.59 ± 0.13	7.79 ± 0.10	7.87 ± 0.10	-0.75 ± 0.84	0.896 ± 0.024
1.5 TPC	7.30 ± 0.13	7.86 ± 0.10	7.81 ± 0.10	-0.39 ± 0.87	0.889 ± 0.026
0.5 in $r\phi$	7.61 ± 0.10	7.84 ± 0.08	7.99 ± 0.08	-0.99 ± 0.77	0.913 ± 0.017
1.5 in $r\phi$	7.29 ± 0.17	7.77 ± 0.12	7.81 ± 0.13	-1.44 ± 0.99	0.859 ± 0.033
0.5 in z	7.60 ± 0.10	7.79 ± 0.09	8.11 ± 0.09	-0.84 ± 0.81	0.915 ± 0.019
1.5 in z	7.48 ± 0.15	7.81 ± 0.11	7.70 ± 0.11	-0.38 ± 0.88	0.874 ± 0.028

Table 4: Stability of the fitted HBT parameters on variation of the cuts for $\pi^+\pi^+$ and p_t over 500 MeV. Standard corresponds to the set listed in Table 3 and TPC anti-merging cut equal 3 cm. See text for details.

p_t range [MeV]	R_o [fm]	R_s [fm]	R_l [fm]	$R_{os}^2[fm^2]$	λ
< 500	0.04	0.03	0.03	0.25	0.025
> 500	0.3	0.2	0.3	0.5	0.05

Table 5: Systematic errors for $\pi^+\pi^+$, defined as the spread of the parameters in Tables 2 and 4

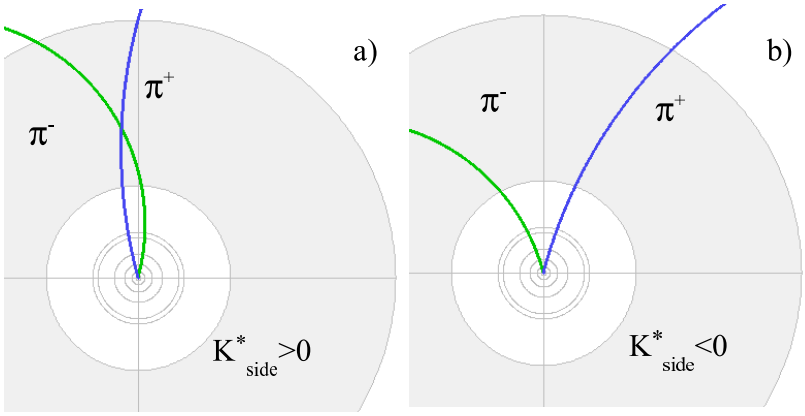

Figure 16: Two possible topologies of track with opposite sign of a charge.

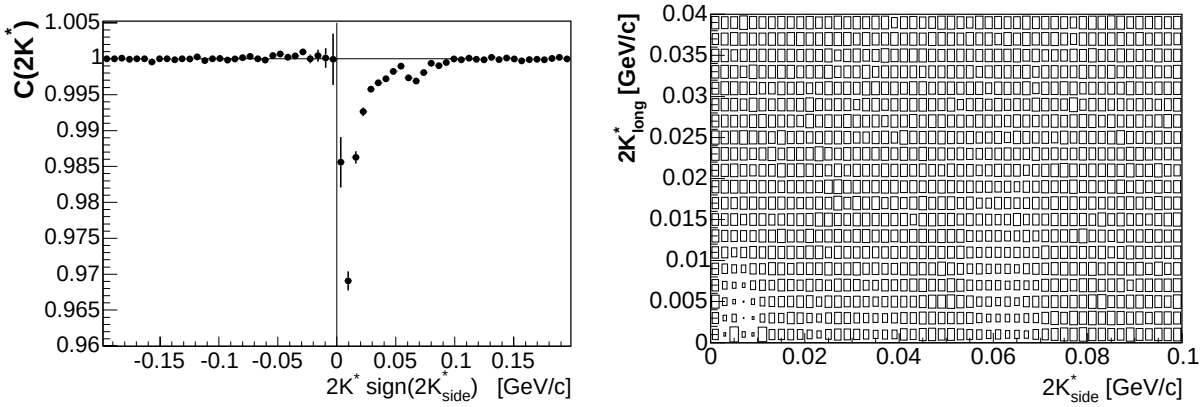

(a) (b)

Figure 17: a) $2K^*$ and b) $2K^*_{side}2K^*_{long}$ for $2K^*_{out} > 0$ correlation functions. $\pi^+\pi^-$ p_t below 500 MeV.

two topologies. One can distinguish them by the sign of $2K^*_{side}$. The measured $2K^*$ correlation function for both, negative and positive $2K^*_{side}$, should be identical due to the symmetry constraint. Hence, a different shape of these functions indicates the presence of the merging.

We have observed the merging effect only for pairs that have positive $2K^*_{side}$, see Fig.17a. It was found that the inefficiencies are related to the cases when two tracks crosses an ITS layer too close to each other. Each of the "deeps" in Fig.17b is associated with the merging at a given layer. The one for $2K^*$ below 20 MeV is related to the pixel detectors, next two - to the drifts, and the last one - to the strips.

Similarly to the $\pi^+\pi^+$ we have decided to apply a cut based on the calculated track separation. In order to asses the the threshold values we have constructed 3D correlation function, $2K^*_{side}$ versus spacial track separation in z and $r\phi$ at a given ITS layer. We have found that the cut with the threshold values listed in Table 6 removes the merging effect. In this case there is no necessity of varying threshold values with transverse momentum because the cut does not have critical impact on statistics in the signal region even for high momentum sample.

Layer	$r\phi$ [mm]	z [mm]
1 (SPD1)	1	1.5
2 (SPD2)	1	1.5
3 (SDD1)	8	5
4 (SDD2)	8	5
5 (SSD1)	20	20
6 (SSD2)	20	20

Table 6: Chosen values of the anti-merging cut in ITS for the low momentum range $\pi^+\pi^-$.

8.3 πK systems

The obtained correlation functions, without any final state effect included in the simulation, are presented in Fig.18. However, the procedure used for the pion systems did not bring the expected result. Increasing the thresholds to large values faster removes all the data points bearing the correlation effect that is expected to be observed (radii of the order of 6 fm and time shift 4 fm), then the merging effect. We must conclude that the closer look into the Kaon reconstruction code is necessary in order to find the source of such a big effect. The observed skews in the residual plots reference to resolution note supports the statement about the imperfection (*vel* bug) of the reconstruction code.

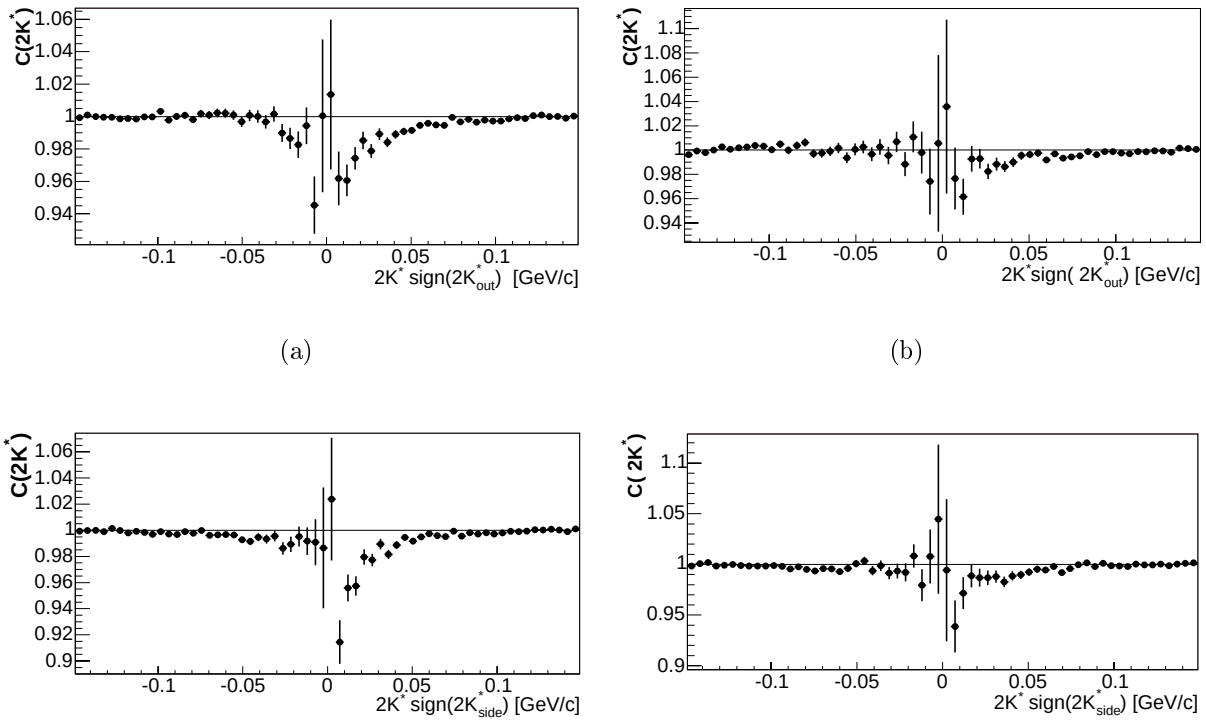

(a) (b)

(c) (d)

Figure 18: Correlation functions for π^+K^+ (left) and π^+K^- (right). No pair cuts applied.

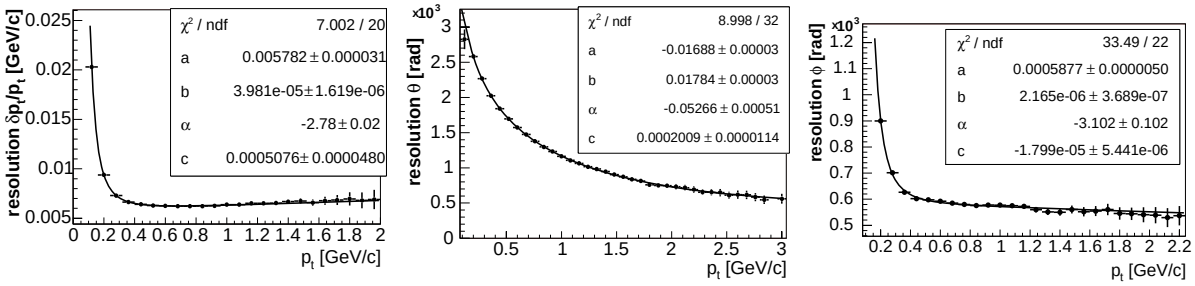

(a) (b) (c)

Figure 19: Resolutions of a) $\delta p_t/p_t$ b) $\delta\theta$ and c) $\delta\phi$ in function of transverse momenta. The lines are the fits to equation (5)

9 Resolution Corrections

Correlation function that we would like to measure (further we will call it *ideal*) is distorted by the finite detector resolution. These distortions lead to the systematic change of the reconstructed HBT parameters. That is why it is necessary to introduce a correction procedure.

We have decided to use the procedure proposed by M.A. Lisa which is applied in the STAR experiment [8]. The idea is based on the fact, that if in equation (4) $C(q)_{meas}$ and $C(q)_{smear}$ are identical, one gets the *ideal* correlation function ($C(q)_{ideal}$).

$$C(q) = C(q)_{meas}\frac{C(q)_{ideal}}{C(q)_{smear}} = \frac{N(q)_{meas}}{D(q)_{meas}}\frac{\frac{N(q)_{ideal}}{D(q)_{ideal}}}{\frac{N(q)_{smear}}{D(q)_{smear}}} \tag{4}$$

$C(q)_{meas}$ and $C(q)_{smear}$ stand from *measured* and *smeared* correlation functions, respectively. The ideal correlation function is obtained using a model form of a correlator (the Gaussian one in the our case). Its numerator and denominator histograms are both constructed from the *mixed* pairs (i.e. originating from different events) but numerator is filled with the weight calculated from the model.

Similarly the smeared correlation function is constructed from mixed pairs but distorted particle momenta are used. Numerator is filled with the same weight as the one of the ideal correlation function (calculated with not smeared momenta).

The tracking reconstructs curvature (i.e. inversed transverse momentum), polar and azimuthal angles. Their distortions in function of p_t are presented in Fig.19. We use the following parametrization of the errors

$$\delta X = a_X + b_X p_t + c_X {p_t}^{\alpha_X}, X = p_t/p_t, \theta, \phi \tag{5}$$

The fitted parameters are presented in Table. 7

X	a	b	c	α
$\delta p_t/p_t$	5.78220e-03	3.98063e-05	5.07594e-04	-2.78008
$\delta\theta$	-1.68773e-02	1.78440e-02	2.00940e-04	-5.26559e-02
$\delta\phi$	5.87693e-04	2.16488e-06	-1.79892e-05	-3.10218

Table 7: The fitted parameters of the error parametrization functions.

Iteration No.	R_o [fm]	R_s [fm]	R_l [fm]	$R^2_{os}[fm^2]$	λ
0	7.90 ± 0.03	7.87 ± 0.02	7.89 ± 0.02	-0.51 ± 0.23	0.923 ± 0.005
1	8.03 ± 0.06	7.88 ± 0.05	7.90 ± 0.05	-0.62 ± 0.51	0.941 ± 0.012
2	8.03 ± 0.03	7.89 ± 0.03	7.91 ± 0.03	-0.63 ± 0.27	0.942 ± 0.006

Table 8: Parameters obtained after resolution correction. p_t below 500 MeV.

The Cartesian momentum components are calculated from the following equations

$$p_x = p_t \cos\phi \quad (6)$$

$$p_y = p_t \sin\phi \quad (7)$$

$$p_z = \frac{p_t}{\tan\theta} \quad (8)$$

so their distortions are

$$\delta p_x = p_x \frac{\delta p_t}{p_t} - p_y \delta\phi \quad (9)$$

$$\delta p_y = p_y \frac{\delta p_t}{p_t} + p_x \delta\phi \quad (10)$$

$$\delta p_z = p_z \frac{\delta p_t}{p_t} + p_t \frac{\delta\theta}{\sin^2\theta} \quad (11)$$

Correction procedure is used in an iterative way and is proven to converge quickly. The starting values of the parameters are obtained from the fit without correction. The change of the fitted parameters in the consecutive iterations is shown in Tables 8 and 9 .

Iteration No.	R_o [fm]	R_s [fm]	R_l [fm]	$R^2_{os}[fm^2]$	λ
0	7.63 ± 0.13	7.78 ± 0.10	7.85 ± 0.10	-0.42 ± 0.85	0.891 ± 0.024
1	7.98 ± 0.16	7.75 ± 0.12	7.85 ± 0.12	-0.51 ± 1.04	0.925 ± 0.030
2	8.03 ± 0.16	7.75 ± 0.12	7.85 ± 0.12	-0.52 ± 1.05	0.928 ± 0.030
3	8.03 ± 0.16	7.75 ± 0.12	7.85 ± 0.12	-0.52 ± 1.04	0.928 ± 0.030

Table 9: Parameters obtained after resolution correction. p_t over 500 MeV.

The most affected parameter is R_{out}, especially for high momentum sample. This is understandable since this component depends linearly on transverse momentum so its resolution also worsens linearly with p_t.

10 Particle Identification

A shape of correlation function is also influenced by the contamination of other particle types then considered ones. In the experimental data analysis the pion pair purity (ratio of the number of correctly identified pions to the number of all particles considered as pions) can be estimated from the product of the particle PID probabilities, which is further referred as the *pair probability*. In Fig.20 there are compared obtained purities and pair probabilities in function of Q_{out}, Q_{side} and Q_{long}.

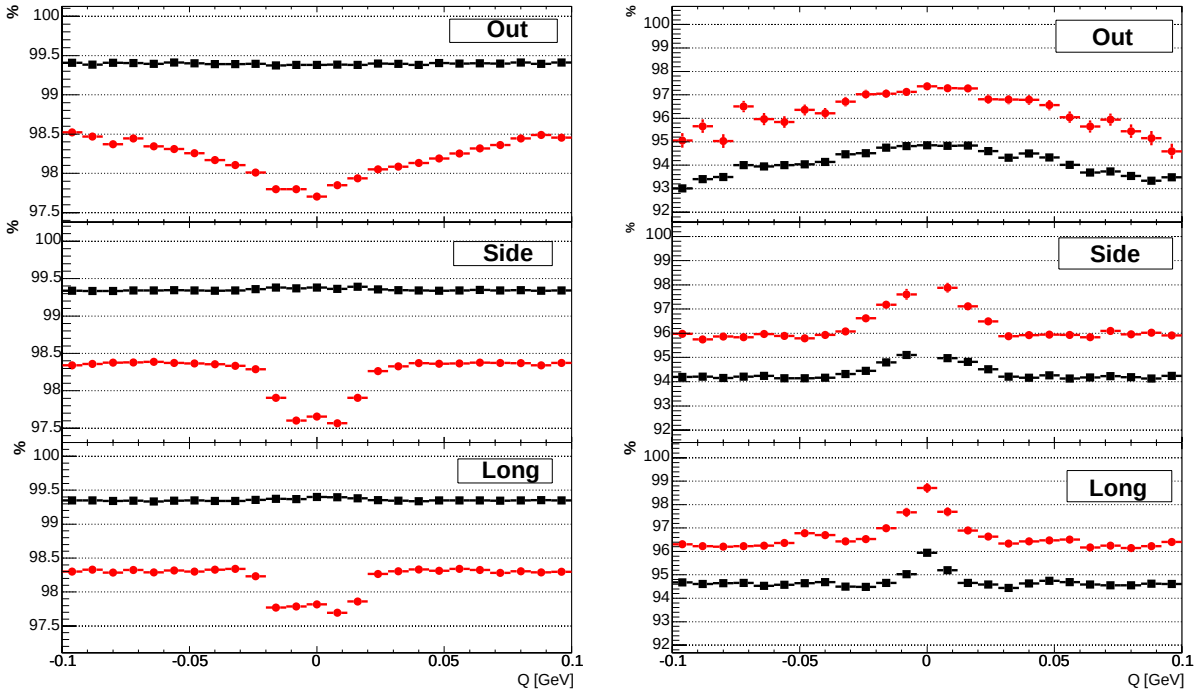

(a) (b)

Figure 20: Pair probability (black squares) and efficiency (red circles) versus Q_{out}, Q_{side} and Q_{long} for $\pi^+\pi^+$ with p_t's a) below and b) over 500 MeV. The plots are constructed by projecting 3D histograms for the absolute values of the other coordinates < 20 MeV. Anti-merging cuts were applied.

The way we simulate correlation effects is based on the weight approach that lets construct correlation functions for the events having no correlations embedded. However, there rises the question if the presence of the correlations modify the performance of the reconstruction. Namely, there might appear an additional dependence of the two particle PID efficiency on relative momentum components if some regions of the phase-space are more (or less) occupied by the pion pairs. To verify that we have generated 500 events using HBT processor after burner. The measured efficiencies were compatible with the

	R_o [fm]	R_s [fm]	R_l [fm]	$R^2_{os}[fm^2]$	λ
Low p_t no corr.	8.03 ± 0.03	7.89 ± 0.03	7.91 ± 0.03	-0.63 ± 0.27	0.942 ± 0.006
Low p_t corrected	8.03 ± 0.03	7.89 ± 0.03	7.91 ± 0.03	-0.62 ± 0.28	0.947 ± 0.006
High p_t no corr.	8.03 ± 0.16	7.75 ± 0.12	7.85 ± 0.12	-0.52 ± 1.04	0.928 ± 0.030
High p_t corrected	8.04 ± 0.16	7.73 ± 0.12	7.85 ± 0.12	-0.54 ± 1.08	0.958 ± 0.032

Table 10: Parameters obtained before and after PID correction.

ones presented in Fig.20.

Particle identification efficiency changes with the transverse momentum. This is the reason of the pair PID efficiency dependence on Q_{out}. Its shape depends on the selected kinematic region of a sample. We have also observed that the anti-merging cut modifies the contamination at small relative momenta. Both of these effects influences the purity of the numerator and denominator exactly the same way.

Unfortunately, pair probability not always follows the PID efficiency. Hence, it is needed to tune the PID reconstruction in order to ensure the best coherence between them.

Correlation functions are corrected in the following way

$$C(Q)_{pidcorr} = (C(Q) - 1)/PID(Q) + 1 \tag{12}$$

where $PID(Q)$ is the PID efficiency function. $PID(Q)$ is created dividing the histogram created the same way as the numerator of a correlation function, but weighted with the pair probability, by the numerator itself. This gives the average PID probability in each bin of a correlation function.

We have found (see Table 10) that the correction has almost no influence on the reconstructed radii and the intercept parameter increases about 2%. Correction made with the real efficiency gives very similar result. It was also verified that the correlation function constructed only with the correctly identified pions gives the coherent result.

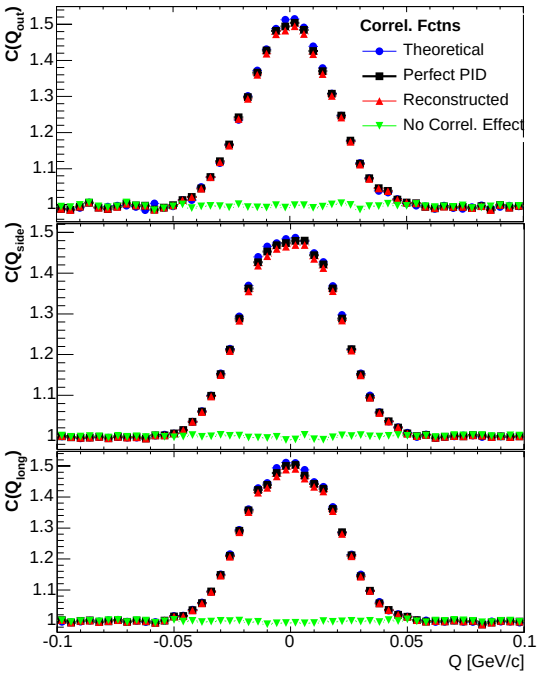

Figure 21: $\pi^+\pi^+$ Q_{out} (top) Q_{side} (center) Q_{long} (down) correlation functions for p_t range below 500 MeV, after anti merging correction. Red up-pointing triangles are the reconstructed functions, black squares are constructed only with having correctly identified PID, blue dots are created using generated momenta and perfect PID, green down-pointing triangles are without simulated Bose-Einstein effect.

11 Correlation Functions

11.1 $\pi^+\pi^+$

The fitted radii are very close the simulated parameters. For p_t range below 0.5 GeV three dimensional fit has given $Q_{out} = 8.03 \pm 0.03$ fm, $Q_{side} = 7.88 \pm 0.03$ fm, $Q_{long} = 8.90 \pm 0.03$ fm and $\lambda = 0.947 \pm 0.006$. The shapes of the reconstructed functions are very close to the simulated ones. In Fig.21 reconstructed correlation functions are compared with the ones obtained using information from the generator. We can see that there is almost no influence of the PID impurity on the shape of the correlation function. The influence of finite resolution can be seen by comparing theoretical correlation function (calculated using simulated momenta and PID) with the reconstructed one.

The non-Gaussian shape of the projections is an artifact related to the anti-merging cut, which removes data points at very small values of the relative momenta. Of course these points are not taken to the projection, however, the calculated average without these points is smaller then if they were available.

For the p_t range over 500 MeV we have obtained after all the corrections Q_{out} =

8.14 ± 0.23 fm, $Q_{side} = 7.90 \pm 0.17$ fm, $Q_{long} = 8.14 \pm 0.17$ fm and $\lambda = 0.942 \pm 0.043$. The remaining discrepancies of the reconstructed parameters are related to the resolution effects.

Using the corrections and the cuts described within this note ALICE is able to reconstruct as large radii as 15 fm (see Figures 22 and 23). The radii presented on these plots are the maximum that we managed to reconstruct, and for the higher values of the simulated radii the fits have not converged.

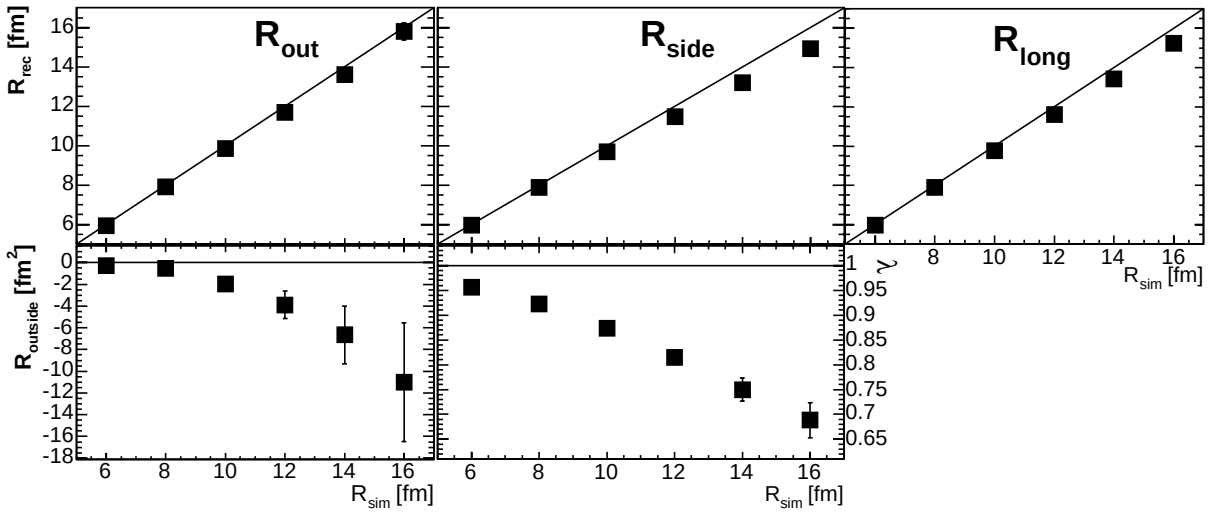

(a)

Figure 22: Extracted source parameters in function of the simulated radii for $\pi^+\pi^+$, p_t below 500 MeV. Only anti-merging cut applied.

11.2 K^+K^+

The available statistics has not allowed for the so detailed analysis of the K^+K^+ correlations and we have been merely able to study 1D case, even when adding together K^+K^+ and K^-K^-. The fitted Q_{inv} correlation function is shown in Fig.24

11.3 $\pi^+\pi^-$

To fit correlation functions of the non-identical particle systems we make use of CorrFit that is described elsewhere in this document. The fitted function is presented in Fig.25. We have simulated radius of 8 fm and time shift 5 fm. Of course we do not expect to observe any time shift in the experimental data. However, since the insufficient statistics has not allowed for the detailed study of pion-kaon nor pion-proton system, we have decided to study this unphysical example.

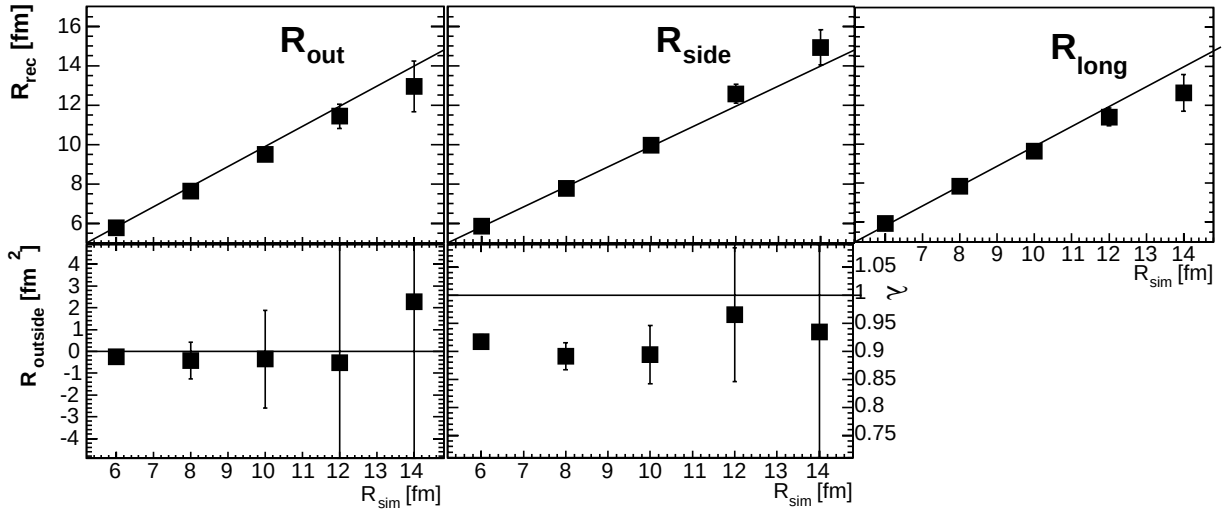

(a)

Figure 23: Extracted source parameters in function of the simulated radii for $\pi^+\pi^+$, p_t over 500 MeV. Only anti-merging cut applied.

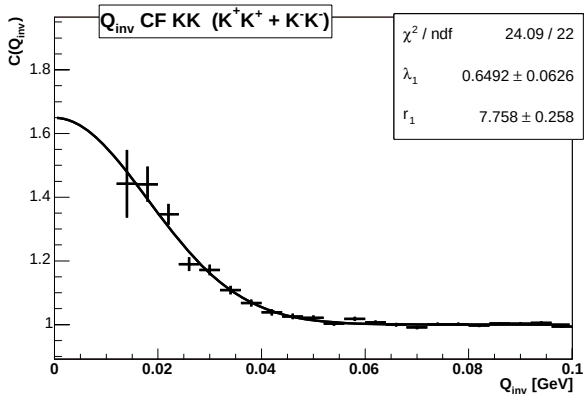

Figure 24: Fitted K^+K^+ (and K^-K^-) Q_{inv} correlation function.

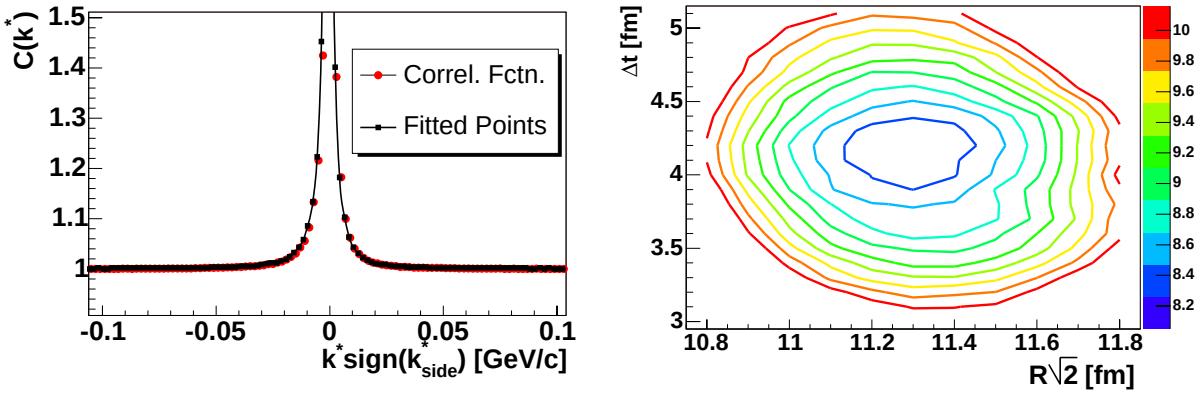

Figure 25: (a) Fitted $\pi^+\pi^-$ correlation function and (b) χ^2 per number of degrees of freedom map of the fit.

The fit has given $R = 7.99$ fm and $\Delta t = 4.3$ fm. The statistical errors can be read from the χ^2 map. The systematical uncertainties are derived from the change of the reconstructed parameters on the variation of the threshold values of the cuts. We have found that they are negligible comparing to the statistical ones and are ~ 0.1 and ~ 0.2 fm for radius and time, respectively.

12 proton-proton collisions

The sizes expected in pp collisions are of the order of 1-2 fm. Hence, the width of the correlation effect is much wider comparing to the Pb-Pb collisions. This, together with the small track density, makes the correlation analyses easier then in the Pb-Pb reactions. In our simulations we have assumed all radii equal to 1 fm, intercept parameter 1 and lack of the final state interactions.

We have used the 10^5 minimum bias events produced during Alice Data Challenge 2004. We have repeated the procedure described for Pb-Pb events. The only obstacle we have encountered were the correlations embedded in the events as produced by the Pythia generator, which are of the non QS origin. The effect increases strongly for the events with very small multiplicity of particles. Hence we decided to consider only events having at least 5 charged tracks reconstructed. The effect is mostly pronounced in Q_{out} and in the consequence it modifies R_{out} by increasing it about 10%.

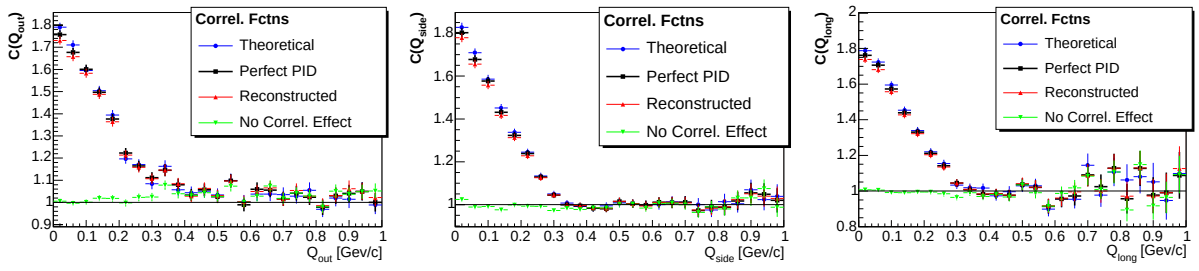

(a) (b) (c)

Figure 26: Projections of the $\pi^+\pi^+$ correlation function for other components smaller then 100 MeV. No cuts applied.

In Fig.26 we show correlation functions without any cuts applied. The merging is almost invisible, however, it is also present. We have applied the same anti-merging cut as for low momentum pions in the case of Pb-Pb collisions. The resulting correlation functions are shown in Fig.27 and the fitted radii are listed in Table 11. The resolution correction was applied, however, it has had no influence on the reconstructed parameters.

The effect of the correlations embedded in the generation level is visible when looking at the correlation function without Bose-Einstein effect in Fig. 26a. The function is clearly not flat. In order to remove the effect we have applied a simple correction, i.e. we have divided obtained correlation function by the one calculated for the events as they are generated by Pythia (without any QS).

The reconstructed radii are basically not sensitive for any changes in the applied cuts. Hence, we can conclude that Alice is able to reconstruct HBT radii with very high precision and the most crucial contribution to the error, and basically the only one, is the systematical one due to the proper handling of the Coulomb and strong interactions.

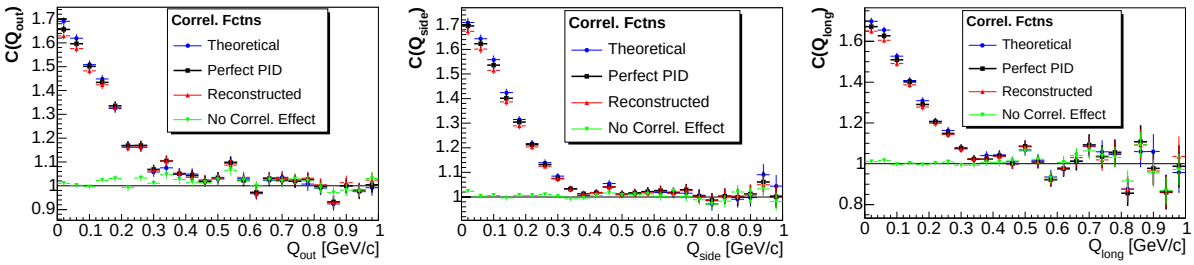

(a) (b) (c)

Figure 27: Projections of the $\pi^+\pi^+$ correlation function for other components smaller then 100 MeV. No cuts applied.

	$R_o[fm]$	$R_s[fm]$	$R_l[fm]$	$R_{os}[fm^2]$	λ
No cuts	0.86 ± 0.03	1.00 ± 0.02	1.03 ± 0.02	0.10 ± 0.05	0.937 ± 0.017
anti-merging	0.90 ± 0.03	0.98 ± 0.02	1.00 ± 0.02	0.07 ± 0.05	0.943 ± 0.019
(*)	0.89 ± 0.07	0.96 ± 0.05	0.99 ± 0.04	0.08 ± 0.12	0.949 ± 0.050
corrected	0.96 ± 0.04	0.97 ± 0.03	0.97 ± 0.02	0.00 ± 0.07	0.908 ± 0.025

Table 11: The reconstructed $\pi^+\pi^+$ radii. (*) anti-merging, PID and resolution corrected

13 Single event interferometry

Analysis of correlation function for single event is important for the studies of the fluctuations phenomena but was practically impossible so far, including experiments at RHIC, due to the lack of the sufficient statistics at the smallest momentum differences of the two-particle (two-pion) systems. Not only the pions multiplicity, but also the effective acceptance resulting from the identification possibilities and the effective track reconstruction at the small relative momenta are important for such analysis.

We have verified the reconstruction efficiency of the Gaussian source with $R_{inv} = 8$ fm, $\lambda = 1$. The demonstrated distributions were obtained for the tracks reconstructed in TPC only. The distributions for the negative and positive pions were added.

The distribution of the fitted radii is presented at the bottom left picture in Fig.28. The Gaussian fit has given the mean value 7.59 fm and $\sigma = 0.63$ fm. The systematic shift of the mean value can be explained as a result of the merging effect and the detector resolution. Neither resolution nor merging can be easily eliminated because they increase significantly already large uncertainty. However, the results indicate the realistic possibilities of ALICE in the single event interferometry analysis, what can be observed on three typical single event correlation functions, where fitted radius and its error are close to simulated value.

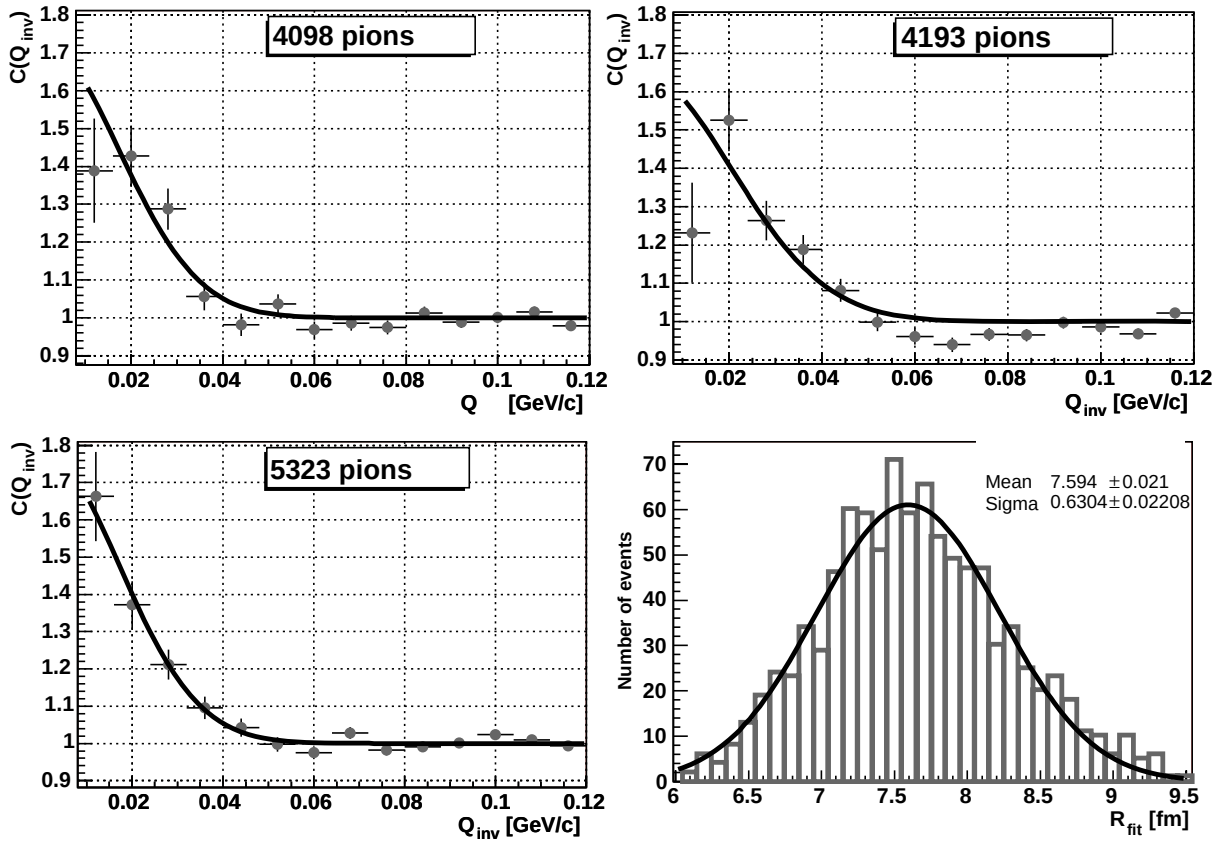

Figure 28: Examples of single event (π^+, π^+) correlation functions for different number of reconstructed pions. Bottom-right: the distribution of the reconstructed radii.

14 Conclusions

We have analyzed PDC04 central events. All the necessary software for HBT analyses has been implemented and it was included to AliRoot. All the detector effects are under control and appropriate tools that let to deal with them have been developed and implemented.

The analysis has shown that ALICE is able to measure the pion HBT radii with the very high precision. The maximum reconstructible radii are around 15 fm are factor 2 larger then currently expected at LHC energies what is a very safe margin.

However, we have discovered that the situation is not so good in the case of the kaon and proton correlations. Although, the reconstruction of these particles is more difficult then pions for the obvious reasons, our simple estimates shows that it should be possible to improve significantly the situation. Hence, the closer look at the reconstruction of the kaons and protons is required.

As an outcome of the presented analyses and the consecutive discussions we find the following points that need to be considered in the future. The appropriate actions need to be undertaken to solve these problems before attempting to analyze the real data.

1. It is essential to be able to preselect events according to their global properties so each job analyzes only similar events. The solution of the STAR experiment, that is based on multiple event buffers, can not be adopted in the our case because of the very large number of bins in z position of the primary vertex. The Offline framework is currently developing the Tag-Database that aims to comply with the requirement. In general, this philosophy of the HBT analysis is the most efficient and error proof. We hope this functionality will be available already for analysis of the next PDC data.

2. Several items could not be done because they require higher statistics then available now. We estimate that 10^5 events with an average $dN_{ch}/d\eta$ of 6000 is sufficient.

   - We would like to study track merging within more bins of p_t (K_t). The best would be to find functional parametrization of the cuts threshold values in function of p_t or K_t. Having that for pions we can assume the same dependence for the other systems and find the appropriate parameters on the basis of smaller number of bins.
   - Azimuthally sensitive HBT for pions. Please note that the information about the simulated event plane vector would be of the great help in this analysis, which is currently not available in Hijing. Hence, it would be useful to add this functionality to the generator or use another one.
   - 3D dimensional analysis for kaons and protons, including resolution and PID corrections study
   - Detailed analysis and systematic error assessment for non identical systems like pion – kaon and pion – proton.

3. The tuning of the tracking is necessary in order to maximize its performance in close track reconstruction efficiency. Especially it is needed for Kaons and Protons.

4. The tuning of the PID reconstruction is required. We hope to be able to use the PID probability as an estimator of the PID efficiency. As it was shown in Section 10 it is certainly not the case at the moment.

References

[1] ALICE Collaboration, Alice Technical Proposal, LHCC-95 (1995)

[2] F. . (. Carminati *et al.* [ALICE Collaboration], J. Phys. G **30** (2004) 1517.

[3] ALICE Collaboration, Computing Technical Design Report

[4] P.K. Skowroński for ALICE Collaboration, physics/0306111.

[5] L. Ray and G.W. Hoffmann. Phys. Rev. **C 54**, 2582 (1996), Phys. Rev. **C60**, 014906 (1999).

[6] http://aliweb.cern.ch/people/skowron/results/PDC04/cent1/index.html

[7] U. W. Heinz, A. Hummel, M. A. Lisa and U. A. Wiedemann, Phys. Rev. C **66** (2002) 044903 [arXiv:nucl-th/0207003].

[8] J. Adams *et al.* [STAR Collaboration], Phys. Rev. C **71** (2005) 044906 [arXiv:nucl-ex/0411036].

[9] R. Lednicky, V.L. Lyuboshitz: Sov. J. Nucl. Phys. **35** (1982) 770; Proc. CORINNE 90, Nantes, France, 1990 (ed. D. Ardouin, World Scientific, 1990) p. 42; Heavy Ion Physics **3** (1996) 93.

[10] A.Kisiel "*CorrFit - a program to fit arbitrary two-particle correlation functions"; NUKLEONIKA* ***49(Suplement 2)*** *(2004) S81-S83*

[11] J. Adams, Phys. Rev. Lett. ***91****, 262302 (2003)*

[12] A.Kisiel (for the STAR Collaboration), Non-identical particle correlations in 130 and 200 AGeV collisions at STAR; J. Phys. G: Nucl. Phys. **30 (2004) S1059-S1063**

[13] ROOT package homepage, *http://root.cern.ch*

[14] Adam Kisiel; *CorrFit program homepage;* `http://hirg.if.pw.edu.pl/ kisiel/CorrFit`